Desalination and Water Treatment
www.deswater.com

doi: 10.5004/dwt.2018.22961

125 (2018) 8–15
September

Multi-parameter analysis of water flows in nanochannels

D. Spetsiotis, F. Sofos, T.E. Karakasidis*, D. Kasiteropoulou, A. Liakopoulos

Laboratory of Hydromechanics and Environmental Engineering, Department of Civil Engineering, School of Engineering, University of Thessaly, 38834 Pedion Areos, Volos, Greece, Tel. +30 24210 74163, email: dimspets@yahoo.com (D. Spetsiotis), Tel. +30 24210 74163, email: fsofos@uth.gr (F. Sofos), Tel. +30 24210 74163, email: thkarak@uth.gr (T.E. Karakasidis), Tel. +30 24210 74163, email: dkasiter@uth.gr (D. Kasiteropoulou), Tel. +30 24210 74111, email: aliakop@uth.gr (A. Liakopoulos)

Received 23 January 2018; Accepted 12 August 2018

ABSTRACT

Water flow simulations play a key role in determining how fluid properties are affected due to geometrical and flow conditions, establishing a theoretical basis so as to guide technological applications of nanofluidics for desalination and water purification. In this work, we investigate liquid water properties when downsizing a Poiseuille-flow system at the nanoscale with Molecular Dynamics simulations. Water is modelled through the well-known SPC and SPC/E models. To establish the theoretical background, we present number density profiles to reveal fluid ordering close to the walls, calculate velocity and temperature profiles for various channel widths and magnitudes of the external driving force and comment on slip length issues. As a multi-parameter study, we aim to contribute on theoretical analysis oriented on water applications design.

Keywords: Water properties; Molecular dynamics; Nanoflows; Nanochannel; SPC model; Slip length

1. Introduction

Examining properties of water at the nanoscale is of particular interest due to water's unique properties and dominant presence in the earth's environment. Research on nanofluidics has increased rapidly during the last years and is suggested for use in a significant number of water-related applications, such as desalination and purification, through nanoparticle incorporation or nanofiltration [1,2]. The key to efficient water treatment systems is the achievement of high fluxes so that nanoscale methods become practical and cost-efficient [3–7]. Where possible, experimental methods could be useful to point out and prove simulation results [8,9].

Molecular dynamics (MD) simulations are among the most popular simulation methods on water investigation. MD can be used for the calculation of fluids in equilibrium (equilibrium MD-EMD) or in fluids that are in non-equilibrium state (non-equilibrium MD-NEMD). Many researchers perform nanofluidic simulations based on simple atomic fluids, based on Lennard-Jones parameters for the ease of computations [10–12] and project their results on water or other molecular fluids. Water simulations have to take into account both interatomic and Coulombic forces in order to extract fluid properties, which might be computationally intensive [13–15]. Apart from pure MD, water properties can be extracted through mesoscale, hybrid and multiscale techniques so as to make it possible to simulate complex systems in terms of substances or geometry [16–19].

Simulations rely on widely accepted water models found in the literature, where different water representations from simple to sophisticated can be found. For the simple point charge (SPC) model, Berendsen et al. in an early work [20] found that the inclusion of a self-energy correction gives an improvement of the effective pair potential of water, while Wu et al. [21] and Paesani et al. [22] introduced terms of flexibility into it. Jorgensen et al. [23] compared six potential functions (BF, SPC, ST2, TIPS2, TIP3P, TIP4P) for simulating liquid water and pointed out the simplicity of SPC, TIPS2, TIP3P models. Improvements on TIP3P model that employ an implementation of Ewald summation to explicitly include long-range electrostatic interactions are presented in [24]. Abascal et al. [25] introduced the TIP4P/2005 general purpose model. In a more recent comparison, Markesteijn et al. [26] showed that the TIP4P/2005 is the

*Corresponding author.

preferred water model on their viscosity calculations, the TIP4P model seems inadequate whereas the SPC/E and TIP4P/Ew models perform moderately. Orsi [27] proposed the coarse-grained ELBA model and found significant computational speed-up on simulations.

Structural and transport properties extracted from MD simulations are to be taken into account when designing water treatment systems. Density profiles reveal fluid layering inside a nanochannel and velocity profiles characterize water transport [28–30]. Water viscocity calculations can be found in [31–33]. Bresme et al. [34] investigated heat transport in liquid water at extreme temperature and pressure conditions, Arismedi et al. [35] calculated the radial distribution function, self-diffusion and viscosity coefficients, while Kunhappan et al. [36] presented calculations on water thermal properties. Confinement in water flows is a significant factor that affects thermal transport and liquid behavior close to the walls differs significantly compared to the bulk liquid. Frank and Drikakis [37] calculated an increase in thermal conductivity values in narrow channels, close to the channel walls, due to the existence of large-scale phonons. Caplan et al. [38] have developed an analytical model which derives the thermal boundary conductance between solids and liquids in terms of surface wettability. Thermal properties of the liquid boundary layer present deviations from the bulk liquid. The study of Ramos-Alvarado et al. [39] revealed a correlation between the interfacial thermal transport and the density depletion length.

The impact of slip on water transport is also of critical importance since it controls transport mechanisms near the solid surface. Surface roughness (thermal, random or periodic) increases shear rates and slip length, as a result [40]. When compared with a smooth one, the rough surface induces extra energy losses and contributes to the reduction of interfacial velocity in nanochannels [41]. Furthermore, fluid flows over rough walls result in formation of irregularly shaped fluid structures around and within the wall cavities [42]. Geometrical characteristics of wall roughness have a different effect on slip length values [43]. Sendner et al. [44] found that the value of the slip length depends sensitively on the surface water interaction strength and the surface roughness. Sega et al. [45] found that a tiny amount of disorder in the atomic positions at the surface is responsible for controlling slip length, while Vinogradova and Belyaev [46] suggest a combination of wetting and roughness to provide better hydrodynamic properties of surfaces.

This work aims to serve as a reference to water properties calculations, such as density, velocity and temperature profiles, and slip length estimation. Carbon channels with atomically smooth surfaces are simulated for various widths and magnitudes of the driving force, for an SPC and an SPC/e water flow model. Simulation details are provided in Section 2, calculated results in Section 3, and the study is summarized in Section 4.

2. Model parameters

Non-Equilibrium molecular dynamics (NEMD) for planar Poiseuille water flow simulation is considered. The computational domain consists of a cubic box, periodic on x- and y-dimensions, with fixed carbon layers that form the upper and the lower wall, each one with 361 particles, while the flow region is filled with water molecules. Walls are set as parallel, flat (more specifically, atomically rough) and stationary surfaces. An external applied force F_{ext} drives the flow at the x-direction. Simulation conditions are summarized in Table 1, where channel height, h, (e.g., distance between the walls) is studied for $15 \le h \le 30$ Å and $F_{ext} = 0.49\ pN$. We also investigate the impact of the magnitude of the external applied force for $0.14 \le F_{ext} \le 0.49\ pN$, while keeping in constant values the channel height $h = 30$ Å, the number of fluid particles $N_f = 891$ and fluid density at $\rho = 0.987$ gr/cm^3. Wall particles are arranged on fcc sites and tether around their equilibrium position due to an applied spring force $F = -K(r(t) - r_{eq})$, where $r(t)$ is the vector position of a wall particle at time t, r_{eq} is its initial lattice position vector and $K = 10$ Kcal/molÅ^2 is the spring constant. Temperature remains constant ($T = 310$K) throughout the simulations. Fig. 1 depicts the periodic model simulated (graphics generated with vmd software [47]).

Lennard-Jones (LJ) parameters are assigned to wall and fluid particles. The LJ potential between two particles i and j is described by the equation

$$u\left(r_{ij}\right) = \begin{cases} 4\mu\left[\left(\dfrac{\sigma}{r_{ij}}\right)^{12} - \left(\dfrac{\sigma}{r_{ij}}\right)^{6}\right], & r_{ij} < r_c \\ 0, & r_{ij} \ge r_c \end{cases} \quad (1)$$

Table 1
Flow parameters for channel height-depended flow ($T = 310$K)

Channel height z-direction (Å)	Fluid density (gr/cm^3)	Number of water molecules
15	0.957	432
20	0.987	594
25	0.969	729
30	0.987	891

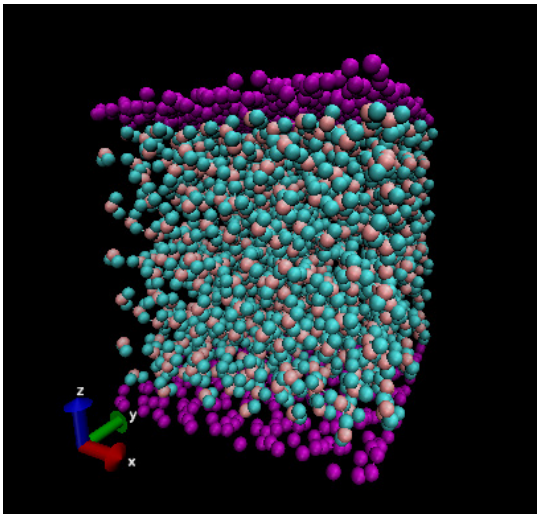

Fig. 1. Carbon channel filled with water.

where parameter ε indicates the interaction strength, σ defines the length scale and r_c the cut-off radius, while the corresponding interatomic force is

$$f_{ij} = \begin{cases} \left(\frac{48\mu}{\tilde{A}^2}\right)\left[\left(\frac{\sigma}{r_{ij}}\right)^{14} - \frac{1}{2}\left(\frac{\sigma}{r_{ij}}\right)^{8}\right], & r_{ij} < r_c \\ 0, & r_{ij} \geq r_c \end{cases} \quad (2)$$

The SPC and SPC/E (extended SPC) water models are simulated here, as choices of simplicity and computational speed. The SPC/E model includes a polarization correction factor that improves the performance of the original SPC model. It was introduced in Berendsen et al. [20] and has been a choice among researchers due to its simplicity, flexibility and close-to-experiment simulation results. Investigations covering available models have shown that the SPC/E is a good choice in terms of computational efficiency and simplicity, although the TIP4P/2005 model seems to be more effective [48].

Water comes as a 3-site rigid molecule with charges and LJ parameters assigned to each of the 3 atoms. Bond and angle styles are harmonic and O and H bonds are fixed in order to form the water molecule. Coulombic interaction between hydrogen and oxygen atoms (carbon atoms are considered uncharged) is given by

$$E = \frac{Cq_iq_j}{er}, \; r < r_c \quad (3)$$

where C is the energy conversion constant, q_i and q_j are charges of atoms and e the dielectric constant. The cut-off radius is r_c = 9 Å for both LJ and Coulombic interactions. Potential parameters for all atomic pairs are summarized in Table 2.

Molecular simulations are performed in LAMMPS [49] using the Verlet time integrator and long range Van der Waals tail correction is taken into account. In the beginning of a simulation, water particles are assigned random initial velocities in order to reach the desired temperature. The system reaches equilibrium state after a run of 2 × 10^6 timesteps (NVT), where the timestep is Δt = 1 fs. Then, external force-driven simulations are performed, where carbon walls follow the NVT ensemble with the application of Nose-Hoover thermostats and water flows under the NVE ensemble, with duration of 5 × 10^6 timesteps and calculated values are averaged.

Table 2
Potential parameters for all atomic pairs

Atom pair	σ(Å)	ε (Kcal/mol)
H–H	0	0
H–O	0	0
O–O	0.1553	3.1660
C–H	0.2530	2.8200
C–O	0.3910	3.1900
C–C	0	0

3. Calculated results

Number density, velocity and temperature profiles and slip length are presented in this Section. Values are calculated at parallel bins along the z-dimension of the channel. The instantaneous water number density is expressed as the number of water molecules located in each bin at a specific time step. This number of atoms is averaged over the total simulation time and a time-averaged value for each bin is extracted. Velocity profiles are created by mean velocities averaged in time at each bin for each time step. Temperature values are also averaged in time in each bin and they are used to construct the temperature profile across the channel. The slip length at the solid boundary, L_s, is generally calculated from the linear Navier boundary condition as $L_s = u_w \Big/ \left.\frac{du}{dz}\right|_w$, where the subscript w denotes quantities evaluated at the wall.

3.1. Density profiles

Density profiles for both SPC and SPC/E water models for channel widths $15 \leq h \leq 30$ (Å) are presented in Fig. 2. For h = 30Å (Fig. 2a) we observe strong fluid ordering in two sharp peaks close to each carbon wall, in a distance of about 8Å from each wall, while the density profile is uniform and constant in the channel interior. There is symmetry of the peaks with respect to the midplane of the channel, while the two innermost peaks have smaller maximum values than the two peaks near the walls. As channel width decreases to h = 25Å (Fig. 2b) and h = 20Å (Fig. 2a), ordering close to the walls still exists and the region of uniformity decreases inside the channels. For the narrowest channel investigated here (h = 15Å, Fig. 2d) it seems that density profile fluctuation spreads across the whole channel. As far as the water model used, no significant differences are obvious between the SPC and SPC/E model, for every channel width.

There is no effect of the external applied force on the density profiles. Figs. 3a–d show that all profiles are identical for the h = 30Å for magnitudes of the external force that varies as $0.21 \leq F_{ext} \leq 0.70$ pN. No difference is observed between the SPC and SPC/E models.

3.2. Velocity profiles

Velocities across the four channels investigated in this work are presented in Figs. 4a–d. Greater velocity values are found in the h = 30Å channel (Fig. 4a) and their maximum value decreases in channels of smaller width, in line, the h = 25Å (Fig. 4b), the h = 20Å (Fig. 4c) and the h = 15Å (Fig. 4d) channel. Second order polynomial functions are applied to velocity values and fit well for the h = 30Å and h = 25Å channels. Parabolic fits for velocity values are not very successful in small channel sizes (h = 20Å and, especially, the h = 15Å channel), where, as we have seen from the respective density profiles, the fluid is strongly homogeneous and the continuum theory breaks down [50–52], but they seem satisfying as channel height increases. Another point worth mentioning is the deviation of maximum velocities between the SPC and the SPC/E model in all cases. We attribute this deviation to the increased shear viscosity employed when the SPC/E model is considered [53].

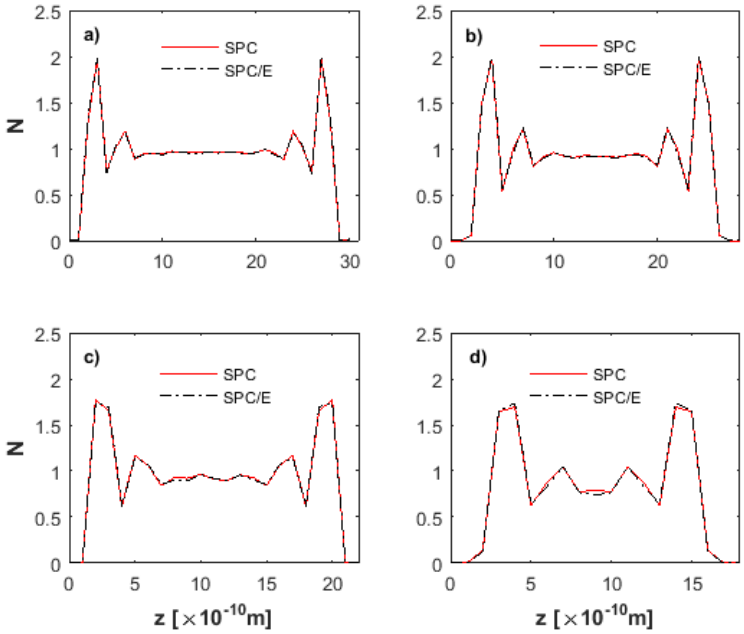

Fig. 2. Density profiles for channels of width a) h = 30 Å, b) h = 25 Å, c) h = 20 Å and d) h = 15 Å (T = 310K and F_{ext} = 0.49 pN).

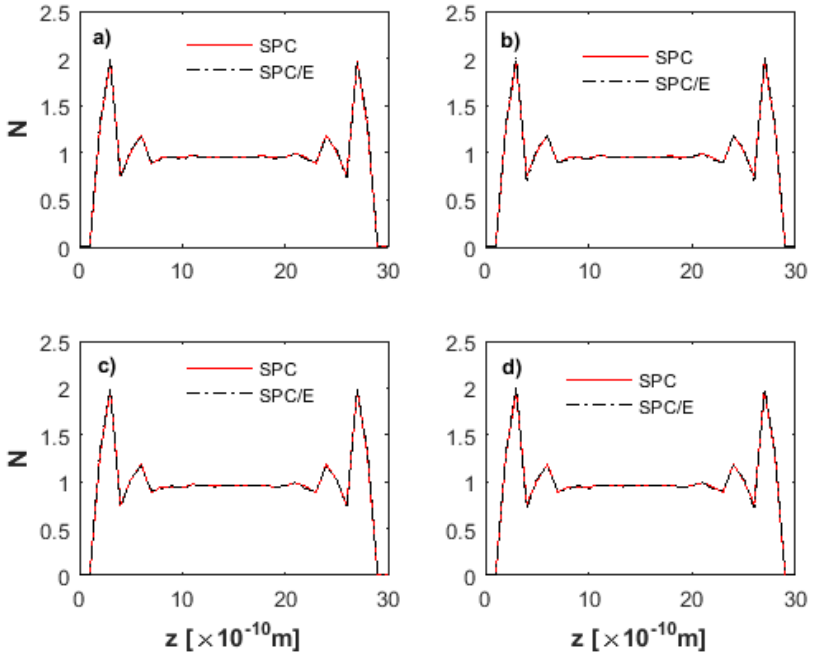

Fig. 3. Density profiles for magnitudes of the external applied force a) F_{ext} = 0.49 pN, b) F_{ext} = 0.35 pN, c) F_{ext} = 0.21 pN, and d) F_{ext} = 0.14 pN (h = 30Å and T = 310K).

When we increase the magnitude of the external force that drives the flow, velocity values across the channels increase, too. Calculated values are presented in Figs. 5a–d for the h = 30Å channel. Velocity profiles deviate from parabolic form as the magnitude of the driving force decreases. Deviation of maximum velocities between the SPC and the SPC/E model is observed in all cases.

3.3. Temperature profiles

In Fig. 6a, the calculated fluid temperature distribution across the h = 30Å channel is presented. At first, we observe that temperature profiles deviate from the expected Navier-Stokes quartic shape [54]. Small deviations occur from the set temperature, especially near the walls, and this

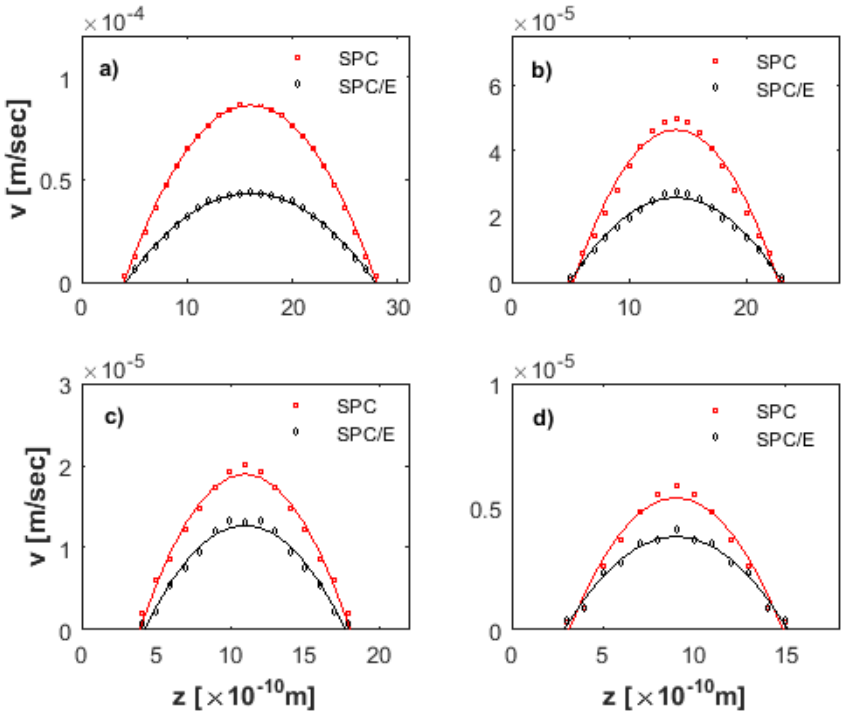

Fig. 4. Velocity profiles for channels of width a) h = 30 Å, b) h = 25 Å, c) h = 20 Å and d) h = 15 Å (T = 310K and F_{ext} = 0.49 pN). Solid lines are 2nd order parabolic fits.

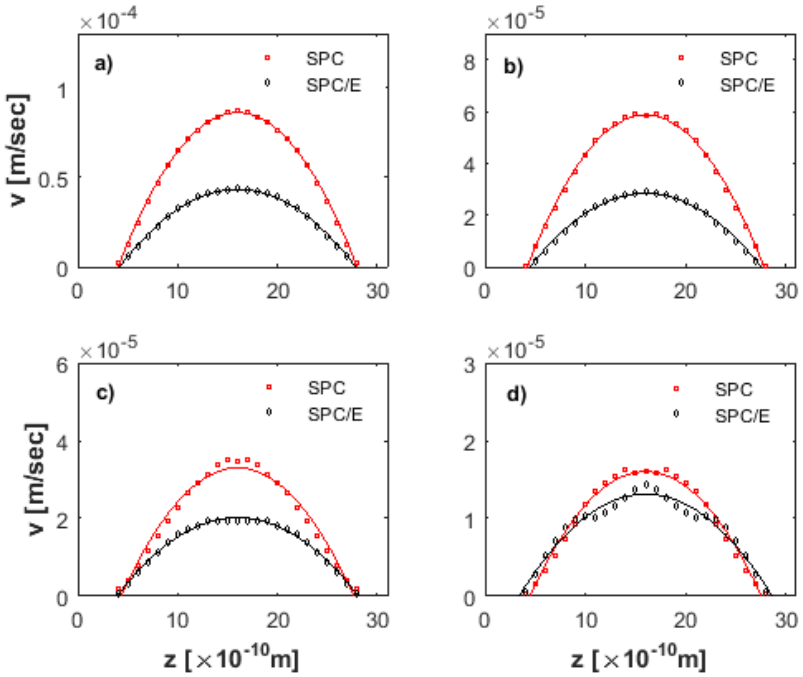

Fig. 5. Velocity profiles for magnitudes of the external applied force force a) F_{ext} = 0.49 pN, b) F_{ext} = 0.35 pN, c) F_{ext} = 0.21 pN and d) F_{ext} = 0.14 pN (h = 30 Å and T = 310K). Solid lines are 2nd order parabolic fits.

could be attributed to discrepancies that appear with the thermostatting mechanism, as has been shown in detail in the work of Bernardi et al. for confined systems with atomic particles [55]. Nevertheless, Nose-Hoover thermostats seem to work well and keep the set temperature in all channels investigated here (Figs. 6b–d).

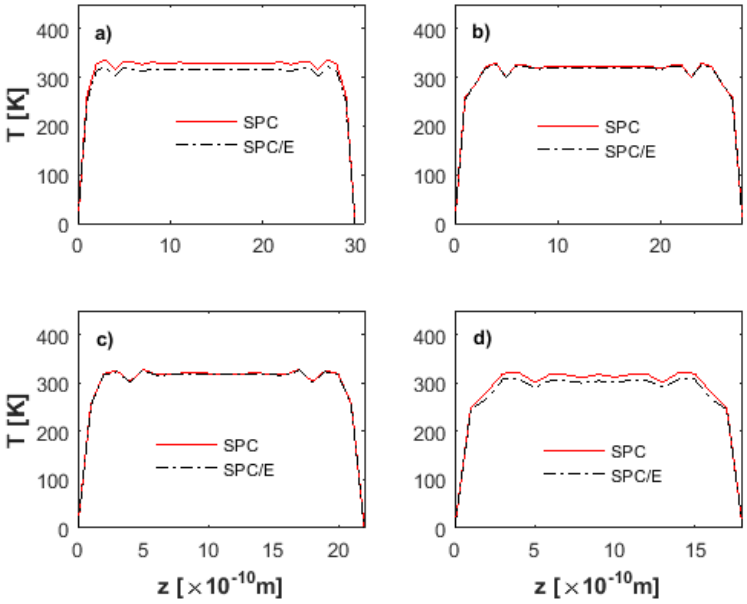

Fig. 6. Temperature profiles for channels of width a) h = 30 Å, b) h = 25 Å, c) h = 20 Å and d) h = 15 Å (target temperature T = 310K and F_{ext} = 0.49 pN). Solid lines are guide to the eye.

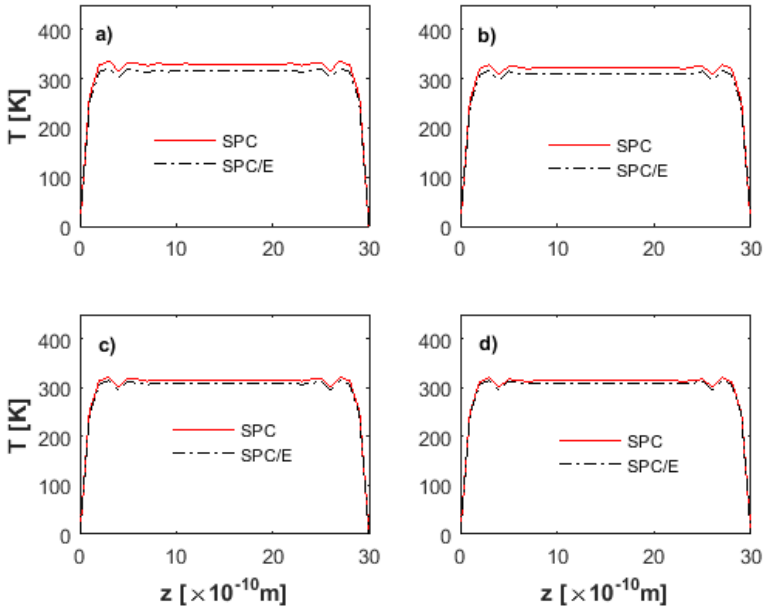

Fig. 7. Temperature profiles for magnitudes of the external applied force a) F_{ext} = 0.49 pN, b) F_{ext} = 0.35 pN, c) F_{ext} = 0.21 pN and d) F_{ext} = 0.14 pN (h = 30 Å and T = 310K). Solid lines are guide to the eye.

Furthermore, when we apply forces of various magnitudes at the h = 30Å channel, we also obtain flat temperature profiles (Figs. 7a–d). Small differences are observed between the SPC and the SPC/E in all cases studied.

3.4. Slip length

Slip length calculations vs. channel width are shown in Fig. 8a. In the channel range investigated here, it is obvious that slip length is maximum at the smallest channel width while it almost reaches its minimum (practically zero) for h = 30Å. Wall effect is maximized at smaller channels and leads to the breakdown of the no-slip condition, as has been addressed by many researchers (the review paper [56] addresses most of the cases). We have noticed similar results in simple monoatomic fluids [57] and now we find that our previous results apply to the combination of liquid water and carbon walls.

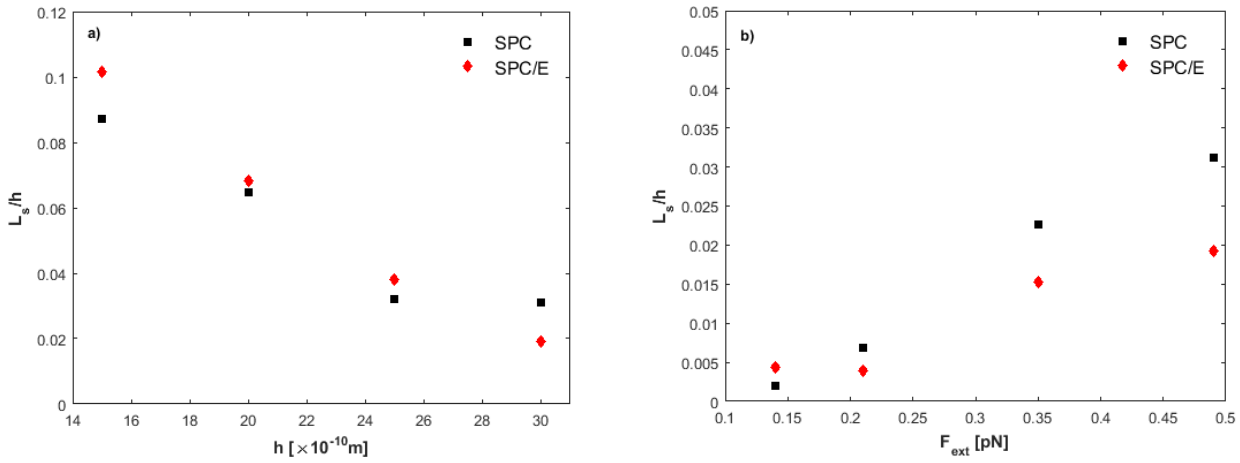

Fig. 8. Slip length at the wall calculated for a) channels between $15 \leq h \leq 30$ (Å) and b) magnitude of the external applied force $0.14 \leq F_{ext} \leq 0.49$ *pN*.

The magnitude of the external applied force, at least in the range investigated here, has a small effect on slip length values (Fig. 8b). As the magnitude increases, slip length increases slightly, though monotonically. Larger forces, with the amount of energy they induce to the flow, seem to force water molecules to slip away from the solid surface of the walls.

Reported slip behavior can be also explained by the work of Niavarani and Priezjev [58]. Shear rates near the channel walls increase when channel dimension decrease or when the external driving force is of high magnitude, and, as a result, the slip length increases.

4. Conclusions

We have presented non-equilibrium molecular dynamics simulations of liquid water flow between atomically-flat carbon walls modeling Poiseuille flow at the nanoscale. The effect of channel width in conjunction with the magnitude of the external driving force was found to affect liquid molecule localization, velocity values inside the channel, temperature distribution and values of the slip length at the wall. By categorizing these flow properties, we wish to contribute on the overall discussion on how reported simulation data can lead the technological design of water flow devices.

The results on water flows presented in this work reveal some of the most important physical properties that one has to bear in mind when designing water flow systems at the nanoscale. It is of importance to point out that previous results found in the literature for monoatomic flows and calculations on structural and transport properties have to be re-examined for respective systems concerning water flows. We believe that electrostatic forces acting between water atoms would alter values in some of the properties (e.g., fluid viscosity), but the trend is to remain the same.

References

[1] N. Savage, M.S. Diallo, Nanomaterials and water purification: Opportunities and challenges, J. Nanopart. Res., 7 (2005) 331–342.
[2] R. Das, Md.E. Ali, S. Bee, A. Hamid, S. Ramakrishna, Z.Z. Chowdhury, Carbon nanotube membranes for water purification: A bright future in water desalination, Desalination, 336 (2014) 97–109.
[3] K. Ritos, D. Mattia, F. Calabrò, J.M. Reese, Flow enhancement in nanotubes of different materials and lengths, J. Chem. Phys., 140 (2014) 014702.
[4] P.S. Goh, A.F. Ismail, B.C. Ng, Carbon nanotubes for desalination: Performance evaluation and current hurdles, Desalination, 308 (2013) 2–14.
[5] J.H. Walther, K. Ritos, E.R. Cruz-Chu, C.M. Megaridis, P. Koumoutsakos, Barriers to superfast water transport in carbon nanotube membranes, Nano Lett., 13 (2013) 1910–1914.
[6] M. Borg, J. Reese, Multiscale simulation of enhanced water flow in nanotubes, MRS Bulletin, 42 (2017) 294–299.
[7] W. Li, W. Wang, Y. Zhang, Y. Yan, P. Kral, J. Zhang, Highly efficient water desalination in carbon nanocones, Carbon, 129 (2018) 374–379.
[8] S.J. Kim, S.H. Ko, K.H. Kang, J. Han, Direct seawater desalination by ion concentration polarization, Nature Nanotech., 5 (2010) 297–301.
[9] J. Li, Y. Long, C. Xu, H. Tian, Y. Wu, F. Zha, Continuous, high-flux and efficient oil/water separation assisted by an integrated system with opposite wettability, Appl. Surf. Sci., 433 (2018) 374–380.
[10] K.P. Travis, K.E. Gubbins, Poiseuille flow of Lennard-Jones fluids in narrow slit pores, J. Chem. Phys., 112 (1999) 1984–1994.
[11] J. Delhommelle, D.J. Evans, Configurational temperature profile in confined fluids. I. Atomic fluid, J. Chem. Phys., 114 (2001) 6229–6235.
[12] F. Sofos, T. Karakasidis, A. Liakopoulos, Non-equilibrium molecular dynamics investigation of parameters affecting planarnanochannel flows, Cont. Eng. Sci., 2 (2009) 283–298.
[13] W.D. Nicholls, M.K. Borg, D.A. Lockerby, J.M. Reese, Water transport through (7,7) carbon nanotubes of different lengths using molecular dynamics, Microfluid. Nanofluid., 12 (2012) 257–264.
[14] J. Su, H. Guo, Effect of nanochannel dimension on the transport of water molecules, J. Phys. Chem. B, 116 (2012) 5925–5932.
[15] A.T. Celebi, M. Barisik, A. Beskok, Surface charge dependent transport of water in graphene nano channels, Microfluid, Nanofluid., 22 (2018) 7.
[16] D. Kasiteropoulou, T.E. Karakasidis, A. Liakopoulos, Dissipative particle pynamics investigation of parameters affecting planar nanochannel flows, Mater. Sci. Eng., B 176 (2010) 176–179.

[17] M. Kalweit, D. Drikakis, Coupling strategies for hybrid molecular-continuum simulation methods, Proc. IMechE Part C: J. Mech. Eng. Sci., 222 (2008) 797–806.
[18] N. Asproulis, D. Drikakis, An artificial neural network based multiscale method for hybrid atomistic-continuum simulations, Microfluid. Nanofluid., 15 (2013) 559–574.
[19] P. Koumoutsakos, Multiscale flow simulations using particles, Annu. Rev. Fluid Mech., 37 (2005) 457–487.
[20] H.J.C. Berendsen, J.R. Grigera, T.P. Straatsma, The missing term in effective pair potentials, J. Phys. Chem., 91 (1987) 6269–6271.
[21] Y. Wu, H.L. Tepper, G.A. Voth, Flexible simple point-charge water model with improved liquid-state properties, J. Chem. Phys., 124 (2006) 024503.
[22] F. Paesani, W. Zhang, D.A. Case, T.E. Cheatham, G.A. Voth, An accurate and simple quantum model for liquid water, J. Chem. Phys., 125 (2006) 184507.
[23] W.L. Jorgensen, J. Chandrasekhar, J.D. Madura, R.W. Impey, M.L. Klein, Comparison of simple potential functions for simulating liquid water, J. Chem. Phys., 79 (1983) 926.
[24] D.J. Price, C.L. Brooks, A modified TIP3P water potential for simulation with Ewald summation, J. Chem. Phys., 121 (2004) 10096.
[25] J.L.F. Abascal, C. Vega, A general purpose model for the condensed phases of water: TIP4P/2005, J. Chem. Phys., 123 (2005) 234505.
[26] A.P. Markesteijn, R. Hartkamp, S. Luding, J. Westerweel, A comparison of the value of viscosity for several water models using Poiseuille flow in a nano-channel, J. Chem. Phys., 136 (2012) 134104.
[27] M. Orsi, Comparative assessment of the ELBA coarse-grained model for water, Mol. Phys., 112 (2014) 1566–1576.
[28] S. Chodankar, E. Perret, K. Nygård, O. Bunk, D.K. Satapathy, R.M. Espinosa Marzal, T.E. Balmer, M. Heuberger, J.F. van der Veen, Density profile of water in nanoslit, Europhys. Lett., 99 (2012) 26001.
[29] F. Sedlmeier, D. Horinek, R.R. Netz, Nanoroughness, intrinsic density profile, and rigidity of the air-water interface, Phys. Rev. Lett., 103 (2009) 136102.
[30] J. Horbach, S. Succi, Lattice-Boltzmann versus molecular dynamics simulation of nanoscale hydrodynamic flows, Phys. Rev. Lett., 96 (2006) 224503.
[31] X.Y. Liu, M.G. He, Y. Zhang, Viscosity of water in the region around the critical point, J. Supercrit. Fluids, 63 (2012) 150–154.
[32] J.S. Medina, R. Prosmiti, P. Villareal, G. Delgado-Barrio, G. Winter, B. Gonzalez, J.V. Aleman, C. Collado, Molecular dynamics simulations of rigid and flexible water models: Temperature dependence of viscosity, Chem. Phys., 388 (2011) 9–18.
[33] G.S. Fanourgakis, J. Medina, R. Prosmiti, Determining the bulk viscosity of rigid water models, J. Phys. Chem., A, 116 (2012) 2564–2570.
[34] F. Bresme, F. Romer, Heat transport in liquid water at extreme pressures: A non equilibrium molecular dynamics study, J. Mol. Liq., 185 (2013) 1–7.
[35] D. Arismendi-Arrieta, J.S. Medina, G.S. Fanourgakis, R. Prosmiti, G. Delgado-Barrio, Simulating liquid water for determining its structural and transport properties, Appl. Radiat. Isot., 83 (2014) 115–121.
[36] K. Deepak, M. Frank, D. Drikakis, N. Asproulis, Thermal properties of a water-copper nanofluid in a graphene channel, J. Comput. Theor. Nanosci., 13 (2016) 79–83.
[37] M. Frank, D. Drikakis, Solid-like heat transfer in confined liquids, Microfluid. Nanofluid., 21 (2017) 148.
[38] M.E. Caplan, A. Giri, P.E. Hopkins, Analytical model for the effects of wetting on the thermal boundary conductance across solid/classical liquid interfaces, J. Chem. Phys., 140 (2014) 154701.
[39] B. Ramos-Alvarado, S. Kumar, G.P. Peterson, Solid-liquid thermal transport and its relationship with wettability and the interfacial liquid structure, J. Phys. Chem. Lett., 7 (2016) 3497–3501.
[40] N.V. Priezjev, Effect of surface roughness on rate-dependent slip in simple fluids, J. Chem. Phys., 127 (2007) 144708.
[41] C. Zhang, Y. Chen, Slip behavior of liquid flow in rough nanochannels, Chem. Eng. Process.: Process Intensif., 85 (2014) 203–208.
[42] N.V. Priezjev, S.M. Troian, Influence of periodic wall roughness on the slip behavior at liquid/solid interfaces: Molecular-scale simulations versus continuum predictions, J. Fluid Mech., 554 (2006) 25–46.
[43] M. Papanikolaou, M. Frank, D. Drikakis, Nanoflow over a fractal surface, Phys. Fluids, 28 (2016) 082001.
[44] C. Sendner, D. Horinek, L. Bocquet, R.R. Netz, Interfacial water at hydrophobic and hydrophilic surfaces: slip, viscosity, and diffusion, Langmuir, 25 (2009) 10768.
[45] M. Sega, M. Sbragaglia, L. Biferale, S. Succi, Regularization of the slip length divergence in water nanoflows by inhomogeneities at the Angstrom scale, Soft. Matter., 9 (2013) 8526–8531.
[46] O.I. Vinogradova, A.V. Belyaev, Wetting, roughness and flow boundary conditions, J. Phys.-Condens Mat., 23 (2011) 184104.
[47] W. Humphrey, A. Dalke, K. Schulten, VMD – visual molecular dynamics, J. Molec. Graphics, 14(1) (1996) 33–38.
[48] C. Vega, J.L.F. Abascal, Simulating water with rigid non-polarizable models: a general perspective, Phys. Chem. Chem. Phys., 13 (2011) 19663–19668.
[49] S. Plimpton, Fast parallel algorithms for short-range molecular dynamics, J. Comput. Phys., 117 (1995) 1–19.
[50] J.S. Hansen, J.T. Ottesen, Molecular dynamics simulations of oscillatory flows in microfluidic channels, Microfluid. Nanofluid., 2 (2006) 301–307.
[51] K.P. Travis, K.E. Gubbins, Poiseuille flow of Lennard-Jones fluids in narrow slit pores, J. Chem. Phys., 112 (2000) 1984–1994.
[52] K.P. Travis, B.D. Todd, D.J. Evans, Departure from Navier-Stokes hydrodynamics in confined liquids, Phys. Rev., E 55 (1997) 4288–4295.
[53] Y. Mao, Y. Zhang, Thermal conductivity, shear viscosity and specific heat of rigid water models, Chem. Phys. Lett., 542 (2012) 37–41.
[54] B.D. Todd, D.J. Evans, Temperature profile for Poiseuille flow, Phys. Rev., E 55 (1997) 2800–2807.
[55] S. Bernardi, B.D. Todd, D.J. Searles, Thermostating highly confined liquids, J. Chem. Phys., 132 (2010) 244706.
[56] B.Y. Cao, J. Sun, M. Chen, Z.Y. Guo, Molecular momentum transport at fluid-solid interfaces in MEMS/NEMS: A review, Int. J. Mol. Sci., 10 (2009) 4638–4706.
[57] F. Sofos, T. Karakasidis, A. Liakopoulos, Parameters affecting slip length at the nanoscale, J. Comput. Theor. Nanosci., 10 (2013) 1–3.
[58] A. Niavarani, N.V. Priezjev, Modeling the combined effect of surface roughness and shear rate on slip flow of simple fluids, Phys. Rev., E81 (2010) 011606.